Fracture Surface Analysis of Optical Fibers

John J. Mecholsky, Department of Materials Science & Engineering, University of Florida

OPTICAL FIBERS are used in many advanced technological applications such as telecommunications, photocopy machines, local military communication systems, sensors, and many more. In these uses, many of the fibers undergo severe loading conditions which require them to be very high in strength. It is therefore very important for them to be as flaw-free as possible. Fractographic analysis is an extremely useful technique for identifying the source(s) of failure and thus help eliminate it (them) during production or fabrication procedures. In addition, fractography can be used to determine the strength and stress state at failure and the time under load before failure.

It is the purpose of this article to demonstrate through examples, how the principles of fracture surface analysis can be applied to research, fabrication, and production problems for strong optical fibers. Although the examples will principally be directed towards optical fibers, the techniques and analyses are valid for most other fibers in different applications, for example, brittle fibers in composites, infrared fibers in various applications and brittle polymer fibers in lighting applications. The fibers that will be presented in this article, in most cases, were intentionally selected for their failure at low loads because the low-strength tail in the strength distribution is the controlling factor in production of long length, strong fibers. It will be shown how observations of the fracture surface can:

- Determine the failure stress
- Identify the size, shape, and type of fracture origin
- Aid in identifying modifications to production procedures to mitigate the flaw severity
- Estimate the time under load

Theoretical Background

Four definitive regions surrounding fracture-initiating flaws in silicate and non-silicate glasses have been observed (Fig 1) (Ref 1–3). The mirror (a flat, smooth region) is bounded by the onset of mist (a region of small radial ridges) which is bounded in turn by

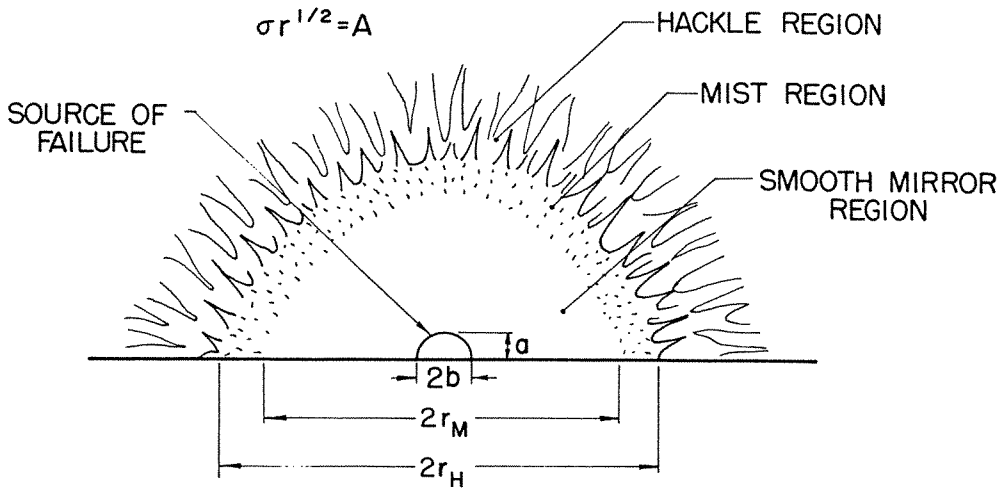

SHAPE AND GENERAL APPEARANCE OF FRACTURE MIRROR SURFACES WITH FLAW.

Fig 1 Schematic of fracture origin showing idealized semielliptical surface flaw and surrounding fracture features known as mirror, mist, and hackle. Crack branching is beyond the hackle.

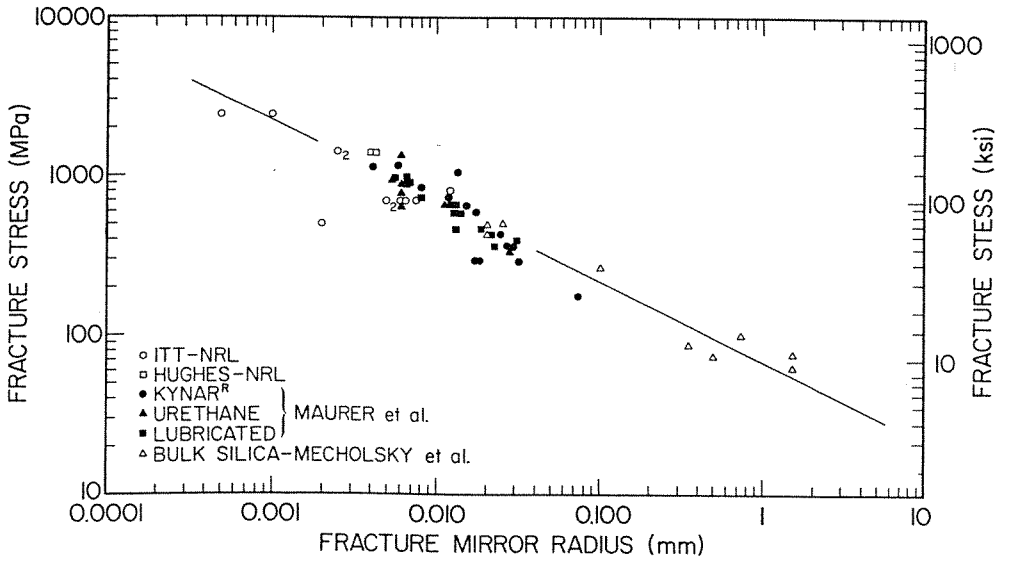

Fig 2 Fracture stress versus inner (mirror-mist) fracture mirror radius for optical fibers and bulk silica. The solid data were obtained from Ref 6 assuming Eq 1 is valid. The bulk silica data are from Ref 3. The other data are from Ref 10. The solid line is a linear least square fit with a slope of −0.5. A_M = 2.1 MPa$\sqrt{m}$.

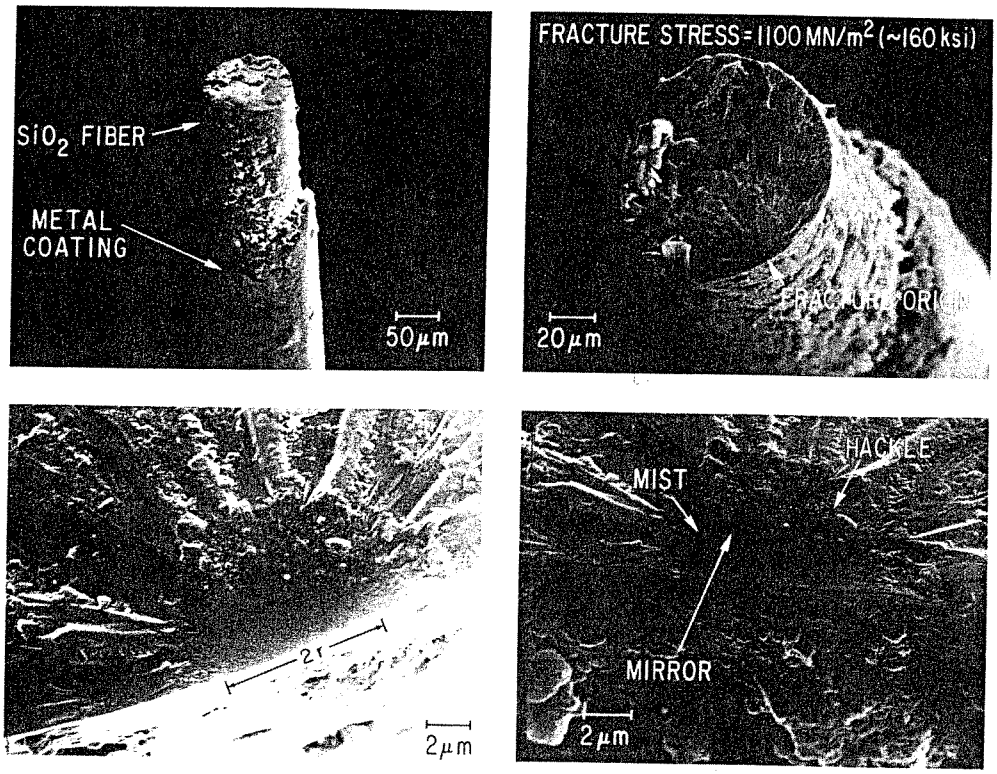

Fig 3 Scanning electron microscope (SEM) fractographs of a metal-coated fiber showing fracture demarcations surrounding the fracture origin (most likely a sharp crack—not visible on the surface)

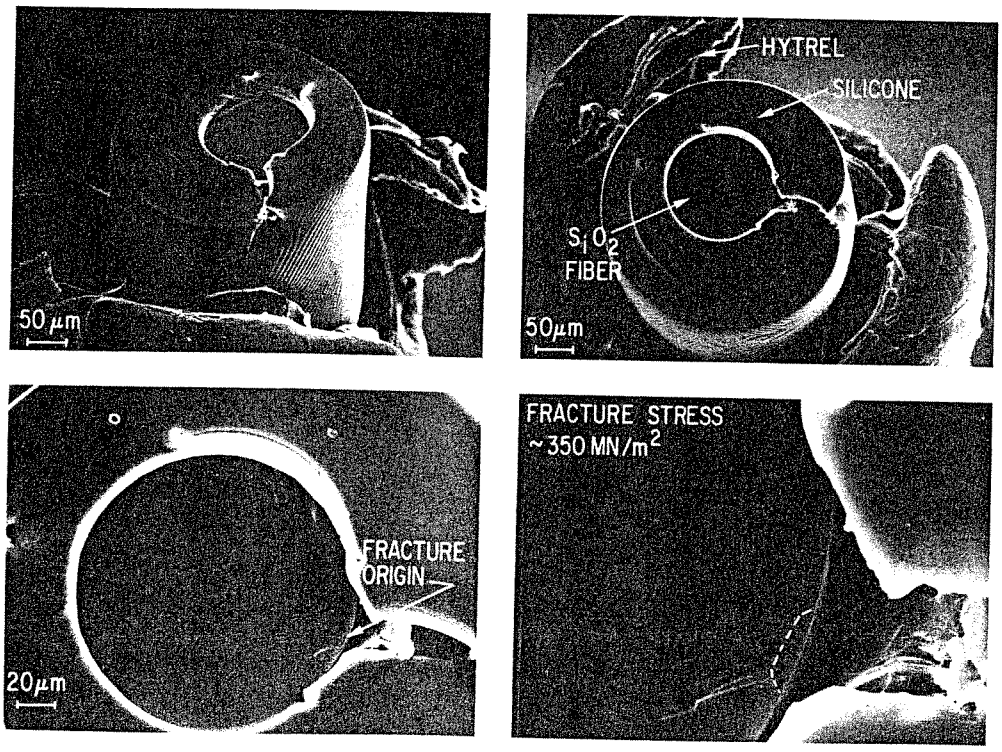

Fig 4 SEM fractographs of a fiber that failed from a sharp crack at the surface (dotted line in lower right fractograph). This fiber failed well below the proof stress of 1400 MPa (200 ksi) indicating failure on the edge of the drum before full stress was achieved.

hackle (a region of larger radial ridges) which is bounded by macroscopic crack branching. In a uniform stress field, these boundaries are circular arcs about the fracture origin. It has been extensively demonstrated that the products of the strength, σ, and the square roots of the distances from the origin to the ons of mist (r_M), the onset of hackle (r_H), and t onset of crack branching (r_B) give three co stant values for silicate glasses:

$$\sigma r_j^{1/2} = A_j \qquad \text{(Eq}$$

where j refers to the mirror-mist, mist-hac le, or crack-branching boundaries. It has be shown that these radii are related to the init flaw depth, a, and half-width, b, through t combination of fracture mechanics and fra ture surface analysis (Ref 3, 4):

$$\frac{c}{r_j} = K_{Ic}^2 Y^2 / 2A_j^2 \qquad \text{(Eq}$$

where $c = \sqrt{ab}$, Y is a factor which depen on the location and geometry of the crack (= 1.12 for a semicircular surface crack), an K_{Ic} is the fracture toughness (0.73 MPa$\sqrt{m}$ or 0.66 ksi$\sqrt{in.}$, for fused silica glass) (R 3). In circumstances where the flaw cann be measured directly, its size can be inferre by that relationship (Ref 5). Even when origin are not macroscopically obvious, fractur markings point back to the area of the origin indicating whether a surface or internal origi was the source of failure. Figure 2 is a grap of fracture stress versus inner mirror/mi boundary radius for fused silica obtained i various studies. The graph shows the validit of Eq 1 over a wide range of stress and mirro radius values. It also indicates that the mirro constant (A_M = 2.1 MPa$\sqrt{m}$, or 1. ksi$\sqrt{in.}$) is the same for bulk fused silica an fused silica fiber. The outer (mist-hackle mirror constant, A_H, is 2.4 MPa$\sqrt{m}$ (2. ksi$\sqrt{in.}$).

An analytical approach to the measuremen of the fracture mirror boundaries was intro duced by Kirchner and Kirchner (Ref 7) and further developed by Kirchner and Conway (Ref 8). This approach assumes that the boundaries of the mirror-mist, mist-hackle and crack branching each occur at a constant stress intensity value, that is, a different branching stress intensity for each boundary. For glasses and polycrystalline ceramics, then

$$K_j = 2Q/(\pi)^{1/2}[\sigma r_j^{1/2}] \qquad \text{(Eq 3)}$$

where σ and r_j are defined as before and K_j is a critical value of the stress intensity, that is, j = 0,1,2,3; for j = 0, $K_0 = K_{Ic}$ and r_0 is the critical crack size (in mode I loading). The j = 0 case is equivalent to the generally accepted fracture mechanics equation for a semicircular surface crack. The value Q is the value necessary to correct K_I for an internal penny shaped crack to obtain the stress intensity factor, K_j, for a semicircular surface crack. Tables are available for these values (Ref 7). The cases of j = 1, 2, and 3 correspond to the formation of the mirror-mist, mist-hackle, and crack-branching boundaries. The set of equations can relate all of the fracture demarcations that we have discussed. Notice that these sets of equations are, in principle, not any different than the previous set presented (Eq 1); however, the above equations

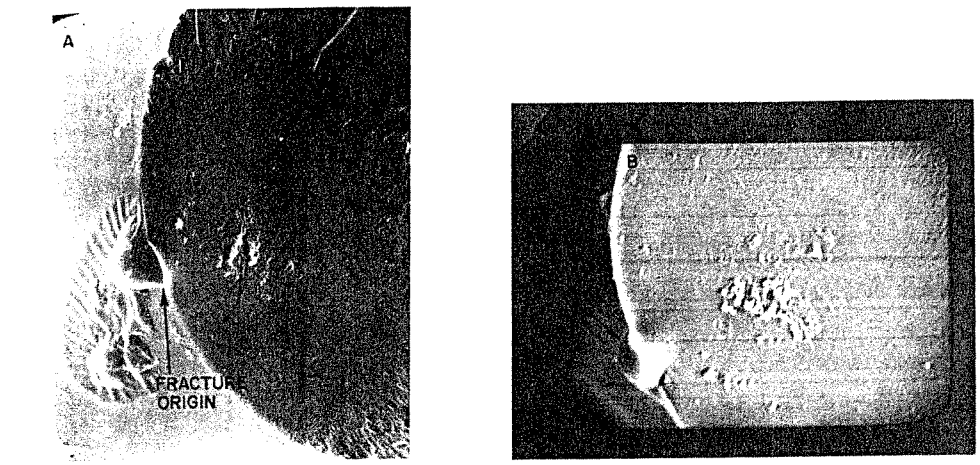

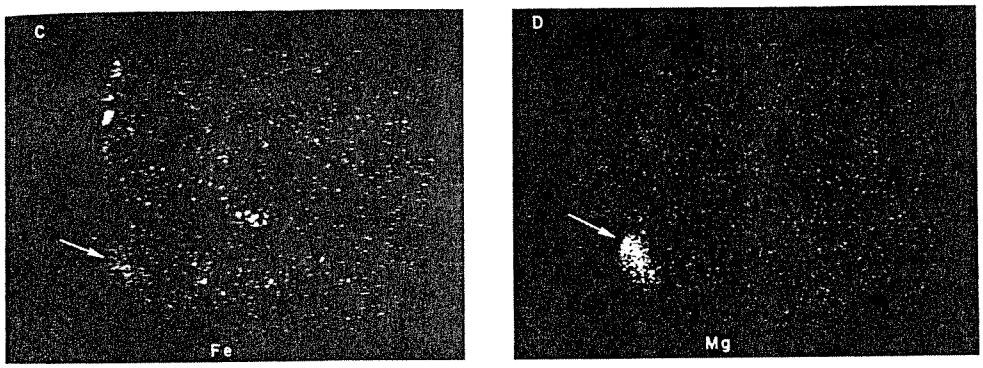

Fig 5 Fiber failure due to a foreign particle. (A) SEM fractograph of a polymer-coated fiber that failed in proof test at 1400 MPa (200 ksi). (B) Real image of A as given by microprobe unit. (C and D) Microprobe electron images showing relative concentrations of Fe and Mg, respectively. Arrows indicate fracture origin (crack between foreign "dust" particle and bulk SiO_2) for reference. The mirror-size measurements indicate a failure stress of ~315 MPa (~45 ksi). This means that this fiber most likely failed before the full proof-stress was achieved, that is, around the edge of the drum.

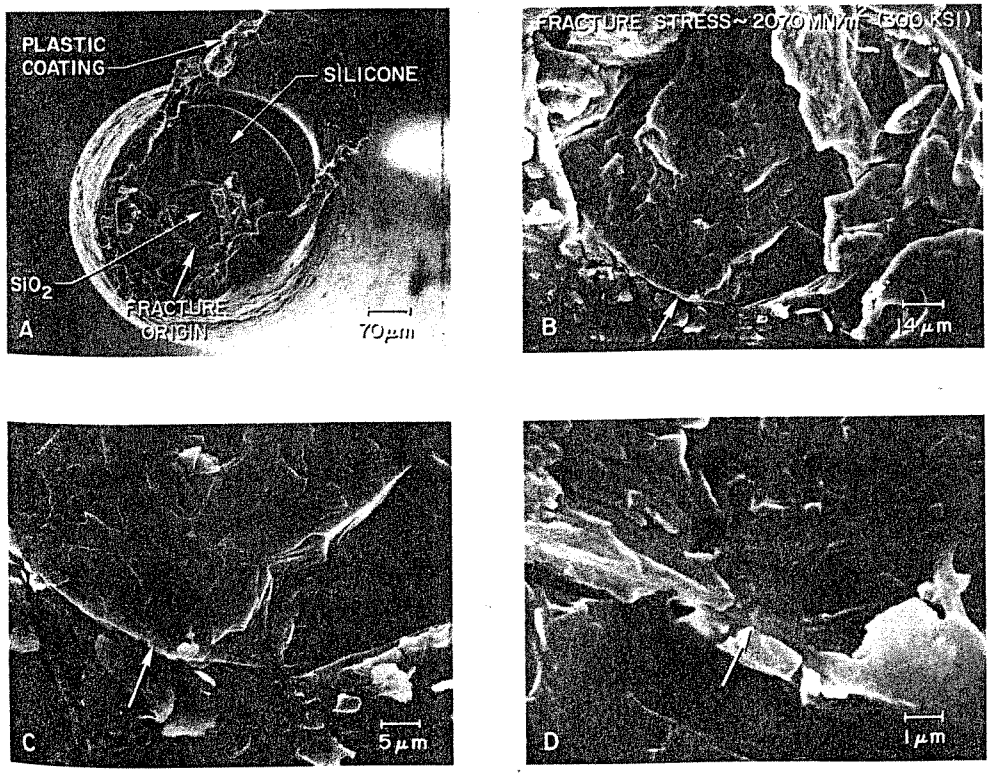

Fig 6 SEM fractographs of a fiber failed from the surface. The nature of the rough area surrounding the origin (arrow in B, C, and D) indicates a high stress (~2700 MPa, or 390 ksi). The exact nature of the fracture origin is unknown, but could be due to a thermal expansion mismatch between two phases (that is, glassy SiO_2 and crystalline SiO_2, or crystalline metal, or crystalline alumina).

are based on well-formulated elasticity equations whereas the previous equations are empirical and only valid along the tensile surface. Also notice that the mirror-to-flaw size ratio naturally evolves from these equations, that is

$$r_1/r_0 = r_1/c = (K_1/K_{1c})^2 = \text{constant} \qquad \text{(Eq 4)}$$

For the sake of completeness, it should be mentioned that Kirchner later modified his approach by requiring a constant strain intensity criterion (Ref 9):

$$K_j/E = \text{constant} \qquad \text{(Eq 5)}$$

where E is the elastic modulus. This will make a difference if single crystals are being analyzed. However, for our purposes there is no difference between Eq 5 and 3.

Experimental Procedure

The polymer-coated fibers used in this study consisted of a silica core with silicone coating and an exterior plastic coating (Hytrel). In order to examine the fractured surface of these fibers, it was sometimes necessary to strip the fiber of the outer Hytrel plastic coating. This was done manually by inserting a razor blade carefully around the fiber and then manually pulling off the severed plastic. The metal-coated fibers contained a metallic (aluminum) coating. When it was necessary to remove this coating, the fibers were placed in an aqua regia solution for 1 to 2 min and then rinsed in water. Before examination in a scanning electron microscope, both types of fibers were coated with gold or platinum.

Three conditions of previously tested fibers were examined. These include delayed failure specimens in which fibers were wrapped around a mandrel and times to failure in air or salt water were measured. This involved merely wrapping fiber around a mandrel of a certain radius. The stress induced in the fiber is related to the mandrel radius. In this case, a fully uniform tensile stress was not achieved, but rather the outer portion of the fiber was in tension and the inner portion of the fiber was in compression. The other conditions of tested fibers were those that were subjected to uniaxial tensile stresses, that is, either proof tested at a particular load or broken in tension on a test machine. Normally, proof testing is done by passing the fiber from one drum to another at a particular rate of speed with a drag on one drum and the load from the drag recorded. Fracture surface observations from

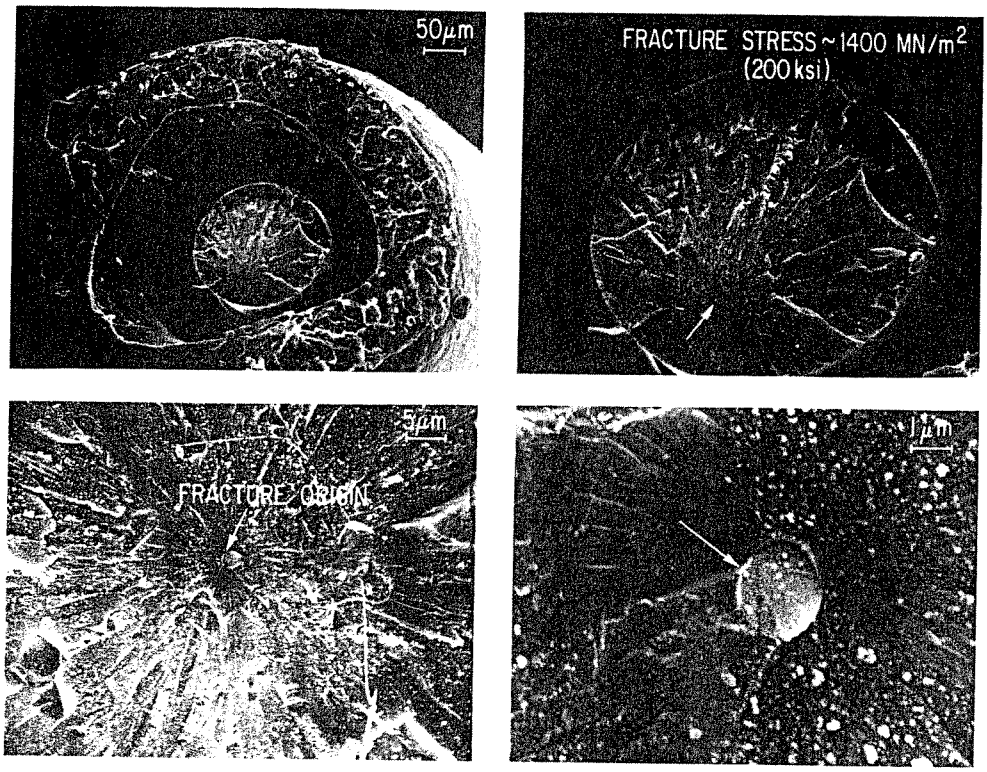

Fig 7 SEM fractographs of a polymer-coated fiber showing failure from a crack at the interface between a rare earth (Nd and La) inclusion and the bulk SiO_2 fiber. The size of the fracture "mirror" region surrounding the origin agrees with the 1400 MPa (200 ksi) proof-stress.

bending or tension tests will be similar and obey Eq 1 to 4 as long as stress-gradient effects are taken into account.

Analysis

More than 100 fibers were analyzed. There are basically two types of fibers that were examined. One type was an aluminum-coated silica-based fiber and the second was a silicone-coated, silica-based glass fiber with an outer organic coating (Hytrel). Since the purpose of this article is to illustrate the usefulness of fractographic analysis and its applications to fiber research, development, and production, only those fibers that illustrate a point will be presented. Further details can be obtained elsewhere (Ref 10).

Stress Analysis. Figure 3 shows a metal-coated fiber that demonstrated the classic mirror, mist, and hackle region schematically represented in Fig 1. The fracture origin in this fiber was most likely a sharp crack that could not be observed; however, by measurement of the mirror-mist boundary, Eq 1 was used to determine the stress (1100 MPa, or 160 ksi) which agreed with that recorded by a load cell. The critical defect size was estimated from Eq 2 to be 0.3 μm. The fiber shown in Fig 4 was fractured in a drum-to-drum proof stress at 1400 MPa (200 ksi). The failure stress inferred from the drag load between the drums and the fiber dimension was 1400 MPa (200 ksi). However, the fracture surface measurements indicate a failure stress of 350 MPa (50 ksi). The difference is apparently due to the fact that failure occurred while that point of the fiber was still in contact with the drum, that is, before it had experienced the full drag load. Without fracture surface examination, it could only be concluded that a stress of 1400 MPa (200 ksi) or less was achieved on fibers failing during proof testing. The main point is that, regardless of the source of loading (mechanical or thermal), in most cases Eq 1 or 3 can be used to determine the stress at failure from the fracture surface.

Flaw Identification. Most of the fracture origins that could be identified (approximately 50) were surface failures. One of the surface failures was a result of a foreign particle (Fig 5A); the remainder resulted from cracks or mechanically induced chips (Fig 4) and "unidentified" sources of failure (Fig 6). It was suspected that at least four of the five fracture origins listed are from small crystallite formations, but this was not determined for certain. The handling or mechanically induced cracks were generally easy to identify and measure (Fig 4). There was generally good correlation between observation and that expected from Eq 1 and 2 (Ref 10).

However, other sources of failure were not as easily analyzed and necessitated other techniques and deductive reasoning. For example, a foreign particle is shown attached to the silica fiber in Fig 5. The flaw severity was not so easy to determine for this attached foreign particle. The particle, which probably attached to the fiber during drawing, caused a small (~2 μm) crack, most likely upon cooling, which subsequently led to failure. The size of this crack is in good agreement with the calculated 3 μm from Eq 2. Chemical analysis by electron microprobe was taken to determine the origin of the particle. That analysis shows the presence of magnesium and iron as well as silica (Fig 5C and D) which implies a dust particle. This type of defect can be avoided by drawing the fibers in a clean room.

Although most fractures were from surface origins, there were seven cases with internal origins. One internal origin was an inclusion containing rare earth elements (neodymium and lanthanum) (Fig 7). This failure occurred due to a (0.2 μm) crack formed between the inclusion and bulk SiO_2. Failure from inclusions related to natural-forming elements can most likely be eliminated by using synthetic quartz material rather than natural quartz. This also applies to preform manufacture used in the chemical vapor deposition (CVD) process. If the outer tube or preform material is natural quartz, then defects such as bubbles and inclusions will be transferred to the final silica fiber. Higher magnification was required to determine the source of these failures because the size of the defect, in most cases, was less than 0.2 μm, and, consequently, detailed analysis was difficult.

Research and Production Aids. In addition to the last two examples given above (Fig 5 and 7), there are two other examples which point out the usefulness of fractography in developing strong optical fibers. One of these cases involves identification of fracture origins in several low-strength fibers. A semielliptical trough on the surface of most of the fibers examined was consistently the location of the failure (Fig 8). Because the ridge along the fiber surface was relatively smooth, it would appear that this defect was produced in the drawing process when the fiber was relatively hot. If the fiber were cool, one would expect a rough gouge if some object were pulled across the surface. Further communications between the failure analysis laboratory and the supplier determined that most probably a ZrO_2 particle adhered to the fiber drawing die orifice and scribed a trough on the hot silica fiber during drawing. The supplier eliminated this type of problem by removing the ZrO_2 tube from the drawing process.

Another example of fracture due to production procedures is shown in Fig 9. Failure is seen to originate at a "bubble" which is one of many along the surface of the fiber. The bubbles along the surface indicate that a large bubble in the preform was drawn out during fiber pulling. The large defect size at the origin (38 μm half width), resulted in

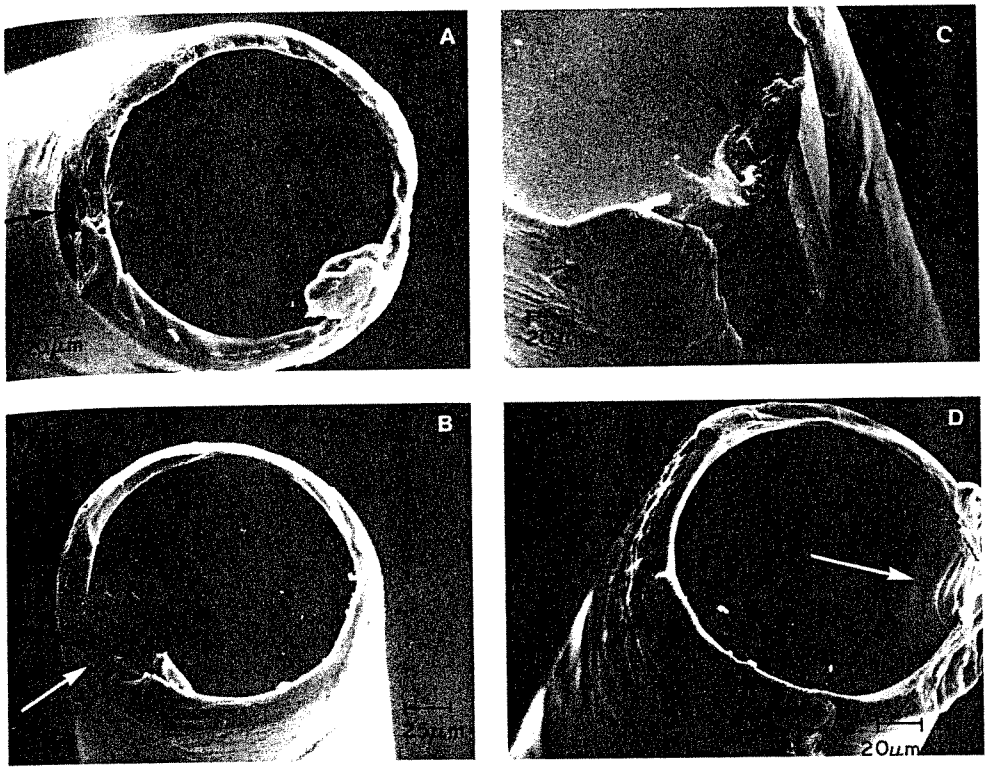

Fig 8 SEM fractographs of four metal-coated fibers failed in a proof test at relatively low strengths. Notice that all fibers indicate surface failure from an elliptical groove with ridge. The smoothness of the depression in B and C would indicate this occurred while the fiber was soft. Also, most likely, the metal is debonded from the fiber in the area around the defect in B and C.

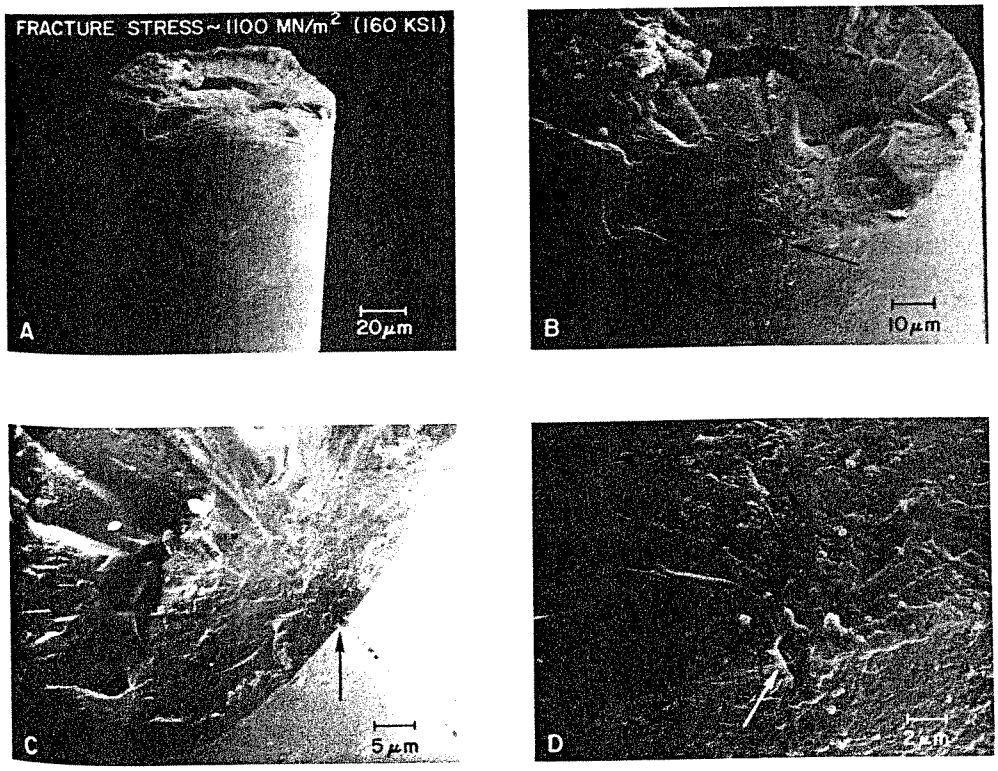

Fig 9 SEM fractographs of a fiber after removal of the metal coating. Source of failure (arrow) is from an elliptical defect, most likely from a bubble in the preform that was drawn out with the fiber.

approximately 1100 MPa (160 ksi) (from mirror-measurements) breaking stress in reasonable agreement with the approximately 1400 MPa (200 ksi) measured during the test. This emphasizes the need for good-quality preforms, if good-quality fibers are to be obtained.

Fractographic Analysis of Subcritical Crack Growth. Many fibers are subjected to subcritical stresses, that is, stresses which do not cause instantaneous failure for a period of time depending on the stress level, initial flaw size, c_i, and time under load, t. These may fail after some extended time under load. This delayed failure results from subcritical crack growth which will subsequently alter the appearance of the fracture surface shown in Fig 1 when failure occurs. The fracture surface produced in delayed failure will show evidence of that subcritical crack growth (Fig 10) where the initial flaw (solid curve) increases until it reaches the critical size (dashed curve) determined by the stress state and fracture toughness, at which time catastrophic fracture commences. The boundaries of the mirror, mist, hackle, and crack-branching regions occur just as they do in catastrophic failure. Thus, the ratio of the initial flaw size to the radius at which the mirror-mist or mist-hackle boundaries form is smaller for a longer time under load. It has been shown for bulk glasses that this was indeed the case both experimentally and theoretically (Ref 11). Only the results will be given here. The time under load and the initial flaw size are related by:

$$\frac{t}{c_i} = \left[\frac{(1.2\pi)^{1/2}}{\phi}\right]^{-n} \frac{(r_j/c_i)^{n/2}}{A_j^n A(1 - n/2)} \qquad \text{(Eq 6)}$$

where n and A are experimentally determined constants which describe subcritical crack propagation velocity (Ref 12) and t is the time under constant stress; r_j and A_j are defined in Eq 1; ϕ is an elliptical integral of the second kind and is a function of the geometry of the crack ($\phi = 1.0$ for a semicircular crack).

Equation 6 demonstrates that, to a reasonable approximation, the mirror radius to initial flaw size ratio should be a function of time under load. In addition, Eq 6 shows that the time to failure can be estimated through fracture surface analysis. A, n, and A_j are constants for a given material, loading, and environment so that measurement of the fracture mirror and initial flaw size can result in a calculation of the time under load. Obviously, this analysis can only be performed after the sample is broken, and thus cannot be used for time-to-failure predictions. However, for in-service failures, given no other information, this is a way to estimate the total time the fiber was subjected to load. An implied assumption is that the stress on the flaw is constant for this period of time. As yet, this analysis has not been tested on fibers, but has been shown valid for bulk glass (Ref 11).

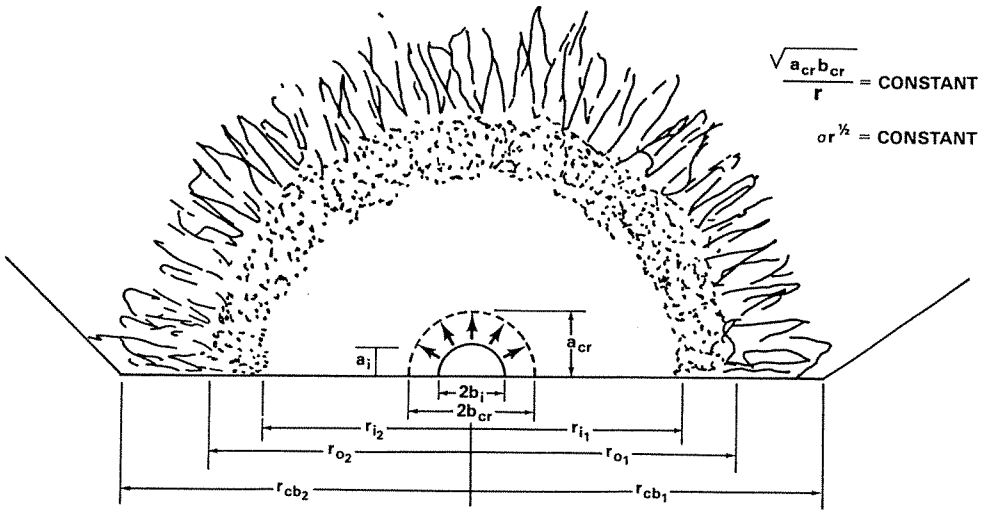

Fig 10 Schematic of fracture surface of a brittle material subjected to a constant subcritical load, σ. The solid semielliptical curve at the center represents the initial flaw size and the dashed curve represents the outline of the critical flaw size before catastrophic failure. The inner, r_i, outer, r_o, and crack branching, r_{cb}, mirror radii are shown in the figure with subscripts 1 and 2 to indicate that there may be unsymmetric mirrors.

Although much research has been devoted to the study of stress corrosion in optical fibers, there are still many questions that remain unanswered, the greatest of which is: Can we predict the service life of fibers in a given environment? Fracture analysis can greatly aid in analyzing long-term results for comparison with theory (Ref 11). Use of fractography where possible in analyzing delayed failure and strain rate experimental results will be invaluable.

Conclusions

Based on the fractographic analysis described in this case history, the following conclusions were drawn:

- Fracture surface analysis can be used to identify sources for the low-strength (or unusual) failures. This knowledge can be used to correct processing or handling procedures to improve the fiber and get a higher yield of "good" fiber
- High-quality glass should be used in all phases of the fiber process
- Most of the low-strength failures of optical fibers are caused by mechanical damage during drawing or defects in the preform (such as bubbles) being drawn through in the fiber process, foreign particle or "stones" from naturally occurring elements or contamination during drawing. One or several of these causes could occur in any run
- The time-to-failure under constant stress may be estimated by observation of the fracture surface

ACKNOWLEDGMENT

The author thanks Dr. S.W. Freiman for much important discussion and encouragement, and S.M. Morey for excellent SEM fractographs. The author acknowledges the support of the Defense Advanced Research Projects Agency (DARPA Order No. 3285), and thanks Hughes Research Laboratory, ITT Research Laboratory, and Naval Ocean System Center, for cooperation in supplying fibers and discussing problems.

REFERENCES

1. E.B. Shand, *J. Am. Ceram. Soc.*, V 42 (No. 10), 1959, p 474–477
2. J.W. Johnson and D.G. Holloway, *Pl los. Mag.*, Vol 14 (No. 130), 1966, 731–743
3. J.J. Mecholsky, R.W. Rice, and S.V Freiman, *J. Am. Ceram. Soc.*, Vol 5 (No. 10), 1974, p 440–443
4. J.J. Mecholsky, S.W. Freiman, and S.M Morey, *Bull. Am. Ceram. Soc.*, Vol 5 (No. 11), 1977, p 1016–1017
5. D.A. Krohn and D.P.H. Hasselman, *Am. Ceram. Soc.*, Vol 54 (No. 8), 197 p 411
6. R.D. Maurer, R.A. Miller, D.D. Smith and J.C. Trondsen, "Optimization c Optical Wave Guides—Strength Stuc ies," ONR contract No. N00014–73-C 0293, Corning Glass Works TR, Ma 1974
7. H.P. Kirchner and J.W. Kirchner, *J. Am Ceram. Soc.*, Vol 62 (No. 3–4), 1979
8. H.P. Kirchner and J.C. Conway, Jr., *J Am. Ceram. Soc.*, Vol 70 (No. 6), 1987 p 413–425
9. H.P. Kirchner, *Eng. Fract. Mech.*, Vo 10, 1978, p 283–288
10. J.J. Mecholsky, S.W. Freiman, and S.M Morey, "Fractographic Analysis of Opti cal Fibers," DARPA Order No. 3285 National Research Laboratory Interin Technical Report from Defense Advance Research Projects Agency, Nov 1977 also, J.J. Mecholsky, S.W. Freiman, an S.M. Morey, Fracture Surface Analysi of Optical Fibers, *Fiber Optics*, B. Ben dow and S.S. Mitra, Ed., Plenum Press 1979, p 187–208
11. J.J. Mecholsky, A.C. Gonzales, and S.W. Freiman, Fractographic Analysis o Delayed Failure in Soda Lime Glass, *J. Am. Ceram. Soc.*, Vol 62 (No. 11–12), 1979
12. S.M. Wiederhorn, *Fracture Mechanics of Ceramics*, Vol 2, R.C. Bradt, D.P.H. Hasselman, and F.F. Lange, Ed., Plenum, 1974